Journal of Electron Spectroscopy and Related Phenomena 200 (2015) 181–192

Contents lists available at ScienceDirect

Journal of Electron Spectroscopy and Related Phenomena

journal homepage: www.elsevier.com/locate/elspec

Quasiparticle band structure

F. Manghi[a,b,*], V. Boni[a]

[a] Dipartimento di Scienze Fisiche, Informatiche e Matematiche, Università di Modena e Reggio Emilia, Via Campi 213/A, I-41125 Modena, Italy
[b] CNR – Institute of NanoSciences – S3, Italy

ARTICLE INFO

Article history:
Available online 5 June 2015

Keywords:
Many-body effects
Hubbard correlation
Photoemission
Quasiparticle states
Highly correlated materials

1. Introduction

Electrons in solids behave in most cases like independent particles, and that in spite of the strong interactions between them. The explanation of this apparent paradox relies on the concept of Landau quasiparticle: the multiple forces acting on one electron dress it up with an interaction cloud and these new dressed particles (quasiparticles) are effectively independent one from the other. A specific tool to investigate the very existence of quasiparticles is photoemission spectroscopy; the time evolution of the system with one removed particle is what is actually measured and when this state evolves as a coherent superposition of oscillations of approximately the same frequency it corresponds to the propagation of a quasiparticle with a reasonably well defined energy and a sufficiently long life-time. In this situation the low-energy excitations of the interacting electrons can be put into a one-to-one correspondence with those of non-interacting electrons with renormalized properties (energy and mass) and the measured spectra can be reduced to a quasiparticle band structure.

From a theoretical point of view, the simplest way to account for e–e interaction is to include it as a mean field where each electron moves independently under the influence of the average charge distribution of all the others. The independent-particle approximation is at very heart of the computational approaches of the band structure of solids. Among these computational approaches, schemes based on the density functional theory (DFT) [1] have proven to be very successful and are by far the most widely used approach for quantitative calculations of realistic systems. Materials for which this rudimentary mean-field description of e–e interaction is sufficient have broad energy bands associated with large values of the kinetic energy of the electrons: this implies that the electrons are highly itinerant and therefore it is reasonable to describe them using a picture in which interactions become smooth and can be averaged out. On the contrary when bands are narrower and the associated kinetic energy smaller, namely when electrons tend to localize around lattice ions, they see each other as individual point charges and the correlation between their motion becomes important. For these systems the single particle picture is inadequate and their electronic properties can be described only treating the multiple pair-wise e–e interaction as a true many-body term.

Strongly correlated electron systems have been one of the most important topics in theoretical solid state research. The major challenge is that the interesting features occur in the regime of intermediate coupling strength, where perturbation theory does not apply. The search for non perturbative approaches has been intense in the last decades, leading now to some widely accepted results, the first one being the choice of the Hubbard model as the general framework to describe strong e–e correlation.

The Hubbard model, where electrons feel their mutual repulsion only when localized on the same site, captures the essential physics of narrow band materials where the itinerant character of valence electrons coexists with strong local correlations responsible of spectroscopic features such as satellites, band-narrowing, and opening, in some cases, of a Mott-Hubbard gap. Traditionally, many-body theories have been formulated for very simple models that are believed to contain the relevant physics of a particular

* Corresponding author at: Dipartimento di Scienze Fisiche, Informatiche e Matematiche, Università di Modena e Reggio Emilia, Via Campi 213/A, I-41125 Modena, Italy. Tel.: +39 3488944680.
E-mail address: franca.manghi@unimore.it (F. Manghi).

http://dx.doi.org/10.1016/j.elspec.2015.05.008
0368-2048/

phenomenon but are very far from true materials; only recently the attention has been devoted to approaches that allow to combine the ideas and methods of many body theory with a realistic description of the system.

A variety of non-perturbative techniques have been proposed during the years to tackle this problem, ranging from dynamical mean field theory (DMFT) [2,3], Gutzwiller variational method on top of local density functional approximation (LDA+G) [4–6], 3-body scattering (3BS) theory [7–11]. In all these method the single particle multi-orbital Hamiltonian is supplemented by the local Coulomb interaction among electrons. LDA+G relies on an ansatz for the ground state wave function where the weight of the energetically unfavored configurations containing double occupancies is reduced. In DMFT the lattice problem of the Hubbard model is mapped onto a single-impurity model embedded in a fermionic bath whose structure has to be determined self-consistently. This mapping is an exact solution of the Hubbard Hamiltonian in the limit of infinite spatial dimensions. The LDA+DMFT scheme is presently implemented in many DFT-band structure packages and is one of the most widely used techniques to compute electronic structures of strongly correlated solids.

In the 3BS approach the interacting many-body state is expanded on the configurations obtained by adding single electron-hole (e-h) pairs to the ground state of the single-particle Hamiltonian. The response of the interacting system to the creation of one hole is then described in terms of interactions between configurations with one hole plus one e-h pair, giving rise to multiple h-h and h-e scattering. The advantage of 3BS with respect to the above mentioned approaches is to provide a rather intuitive interpretation of the effect of electron correlation on one electron removal energies in terms of Auger-like relaxations. In the following we will mainly concentrate on this approach, presenting in some detail the underlying theory. Interestingly the results of DMFT and 3BS in many cases are quantitatively very similar, as we will show.

Among the non-perturbative methods that are used to augment band structure with on-site correlations, schemes based on cluster formalisms are worth mentioning. These so-called quantum cluster (QC) theories [12] share the basic idea to solve the problem of many interacting electrons in an extended lattice by a *divide-et-impera* strategy, namely solving first the many body problem in a subsystem of finite size and then embedding it within the infinite medium. The embedding procedure can be variationally optimized as in the dynamical cluster approach [13] and cellular dynamical mean field theory (CDMFT) [14,15]. Even neglecting self-consistency in the embedding procedure the method, that in this case has been called cluster perturbation theory (CPT)[16,17], gives access to non trivial many body effects, reproducing exactly both the limit $U/t=0$ (non-interacting band limit) and $U/t=\infty$ (atomic limit); for intermediate values of U/t CPT opens a gap in metallic systems at half occupation [17,18]. QC approaches account for the momentum dependence of many-body corrections (self-energies) more appropriately than DMFT or 3BS and for this reason they should provide a more accurate description of quasiparticle dispersion. However QC approaches have been mostly applied to model systems and only few quasiparticle calculations for realistic systems have been reported up to now [19,20].

We will restrict to the simplest examples of materials where e–e correlation plays a crucial role, namely transition metals and transition metals mono-oxides. The article is organized as follows: in Section 2 we will introduce the essential many body concepts and the details of 3BS theory. This will allow us to clearly identify the dependence of correlation effects on band occupation and on spin-polarization. The results for transition metals and transition metal oxides will be presented in Section 3. Section 4 is devoted to open problems and outlook.

2. Beyond the one-electron picture

2.1. Basic many-body concepts

The starting point is the generalized Hubbard Model described by the Hamiltonian where electrons are itinerant – they hop from site to site and are characterized by a band structure dispersion – but at the same time experience mutual repulsion when localized on the same site

$$\hat{H} = \sum_{i\alpha\sigma} \epsilon_{i\alpha} \hat{n}_{i\alpha\sigma} + \sum_{\alpha\beta\sigma} \sum_{ij}{}' t_{i\alpha,j\beta} \hat{c}^{\dagger}_{i\alpha\sigma} \hat{c}_{j\beta\sigma} + \frac{1}{2} \sum_{\alpha\beta} \left[\sum_{i} (U_{\alpha\beta} - J_{\alpha\beta}) \sum_{\sigma} \hat{n}_{i\alpha\sigma} \hat{n}_{i\beta\sigma} + \sum_{i} U_{\alpha\beta} \sum_{\sigma} \hat{n}_{i\alpha\sigma} \hat{n}_{i\beta-\sigma} \right] \quad (1)$$

with $\hat{n}_{i\alpha\sigma} = \hat{c}^{\dagger}_{i\alpha\sigma} \hat{c}_{i\alpha\sigma}$ and $\hat{c}_{i\alpha\sigma}, \hat{c}^{\dagger}_{i\alpha\sigma}$ destruction and creation operators. Here $\epsilon_{i\alpha}$ and $t_{i\alpha,j\beta}$ are the intra- and inter-atomic matrix elements of the one-particle Hamiltonian and $U_{\alpha\beta}, J_{\alpha\beta}$ are on-site Coulomb and exchange terms. Notice that for a single orbital $U=J$ and Hamiltonian (1) reduces to the standard Hubbard model where only electrons of opposite spin experience an on-site repulsion.

We are interested in the excitation energies of the system when an electron is either removed (like in a photoemission experiment) or added (like in inverse photoemission). These excitation energies correspond to differences between energies of the extended system with a variable number of particles, namely $E_0^N - E_n^{N-1}$ and $E_n^{N+1} - E_0^N$ respectively, where E_0^N is the ground state energy of N interacting electrons and $E_n^{N\pm1}$ is any excited state of the same system with one particle added/removed.

In the absence of e–e interaction, these total energies are a sum of single particle eigenvalues and the excitation energies trivially correspond to individual single particle eigenvalues. This is no more true for interacting systems. In this case the excitation energies are obtained, according to many-body theory, as the poles of the one-particle Green's function describing the propagation of an added/removed electron

$$G(k,\omega) = \frac{1}{\omega - \epsilon_k^n - \Sigma(k,\omega)} \quad (2)$$

Here ϵ_k^n are the single-particle band energies and $\Sigma(k,\omega)$ is the self-energy correction to them. It embodies all many-body interactions and is the quantity to be calculated.

The poles of $G(k,\omega)$ occur at $\omega = \epsilon_k^n + \Sigma(k,\omega)$. Since self-energy turns out to be a complex function its effect is twofold: its real part shifts the energy position of the quasiparticle excitations (the band eigenvalues that are in this sense "renormalized" by the interaction) and its imaginary part gives a finite life-time to them. Only long-lived excitations correspond effectively to quasiparticle excitations and appear as sharp maxima of the spectral function

$$A(k,\omega) \equiv \frac{1}{\pi} ImG(k,\omega) \quad (3)$$

On the contrary when the poles occur far from the real axis, the life-time of the excitation is short, the spectral weight is spread out on a large energy window and no quasiparticle – no long lived-excitation – exists any more. These two opposite situations, corresponding to *quasiparticle renormalization* and *quasiparticle quenching*, are illustrated in Fig. 1.

The calculation of self-energy requires inevitably approximations. In order to define them it is useful to consider other exact representations of the one-particle Green's function. The Lehman

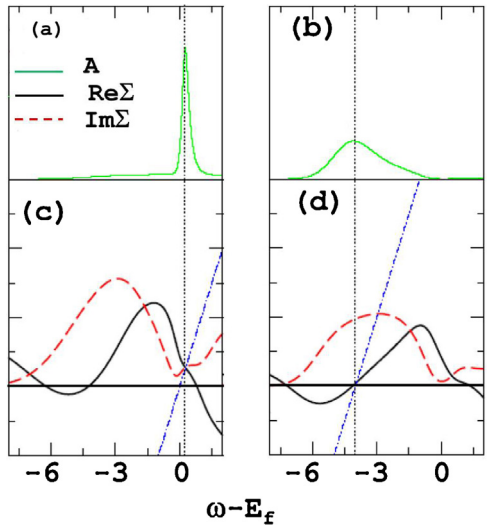

Fig. 1. Illustrative examples of self-energy (black continuous line for real part, red dotted line for imaginary part) and spectral functions (green line). The straight line $\omega - \epsilon^n_{k,\sigma}$ is reported as a blue dotted line; its intersection with the curve $Re(\Sigma(k, \omega, \sigma))$ indicates the energy position of the Green's function pole (see text). Panels (a) and (c) correspond quasiparticle renormalization and to a sharp peak in spectral function. Panels (b) and (d) to quasiparticle quenching. (For interpretation of the references to color in this figure legend, the reader is referred to the web version of the article.)

representation is one of them, involving hole and particle propagators G^-, G^+

$$G(k,\omega) = G^-(k,\omega) + G^+(k,\omega) \tag{4}$$

where

$$\begin{aligned} G^-(k,\omega) &\equiv \sum_n \frac{|<\Psi_n^{N-1}(-k)|\hat{c}_k|\Psi_0^N>|^2}{\omega - (E_0^N - E_n^{N-1}) - i\delta} \\ G^+(k,\omega) &\equiv \sum_n \frac{|<\Psi_0^N|\hat{c}_k|\Psi_n^{N+1}>|^2}{\omega - (E_n^{N+1} - E_0^N) + i\delta} \end{aligned} \tag{5}$$

or equivalently

$$\begin{aligned} G^-(k,\omega) &= <\Psi_0^N|\hat{c}_k^\dagger \frac{1}{-\omega + E_0^N + i\delta - \hat{H}}\hat{c}_k|\Psi_0^N> \\ G^+(k,\omega) &= <\Psi_0^N|\hat{c}_k \frac{1}{\omega + E_0^N + i\delta - \hat{H}}\hat{c}_k^\dagger|\Psi_0^N> . \end{aligned} \tag{6}$$

Here $|\Psi_0^N>$ is the exact – and unknown – ground state of the N-particle interacting system. Notice that according to (6) the hole and particle propagators are the expectation values of the *resolvent* $\hat{G} \equiv 1/z - \hat{H}$ over $\hat{c}_k|\Psi_0^N>$ and $\hat{c}_k^\dagger|\Psi_0^N>$ respectively. In order to transform the exact representations (4)–(6) into useful formulas to calculate Green's function propagators we need to introduce approximate forms of $|\Psi_0^N>$. This will be done in the next section.

2.2. 3BS approximation

The starting point of 3BS approach is the expansion of the interacting N-particle ground state $|\Psi_0^N>$ in terms of (all, in principle) excited states of the corresponding non interacting system (Fig. 2). The main approximation is then to truncate this expansion including just one electron–hole pair. (For extensions of the configuration-interaction scheme to more electron–hole pairs see [21]). This amounts to say that the collection of states

$$\left\{|0>; |d>\right\} \quad \text{where} \quad |0> \equiv |\Psi_0^N> \quad |d> \equiv \hat{c}_{q_2}^\dagger \hat{c}_{q_1}|0>$$

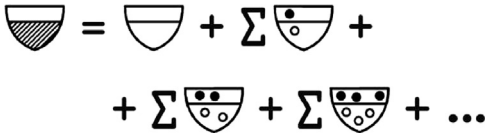

Fig. 2. Pictorial representation of the configuration-interaction expansion of a many-body state Ψ_0^N. The dashed area represents the interacting electrons; the same blank area the non interacting Fermi sea; empty and filled circles denote respectively single hole and electron states.

is a complete basis set for the Fock space of N interacting particle. Correspondingly, the basis set of the Fock space for $N-1$ particles will include up to 3-particle configurations

$$\{|u>; |t>\} \quad \text{where} \quad |u> \equiv \hat{c}_k|0> \quad |t> \equiv \hat{c}_{q_3}^\dagger \hat{c}_{q_2}\hat{c}_{q_1}|0>$$

and the quantum states describing the system with one removed electron are not simply obtained by adding a hole to the Fermi sea ($|u>$) but they are a more complex combination involving also excited states ($|t>$). In terms of physical intuition this means that the removal of one electron is followed by a swarm of shake-up processes corresponding to configurations with one electron–hole pair added. The effects of electron correlation on one-electron removal energies from a partially filled band is then described in terms of interactions between 3-particle configurations giving rise to hole–hole and hole–electron multiple scatterings (Fig. 3).

More precisely the interactions between the 3-body configurations are represented by a set of scattering T-matrices $T^{\alpha\beta}_{\text{h–h}}$ and $T^{\alpha\beta}_{\text{h–e}}$, describing hole–hole and electron–hole scattering respectively. For a majority spin hole we have

$$T^{\alpha\beta}_{\text{h–h}}(\omega) = \frac{U}{1 + U g_3^{\alpha\beta}(\omega)} \tag{7}$$

$$T^{\alpha\beta}_{\text{h–e}}(\omega) = \frac{-U}{1 - U g_1^{\alpha\beta}(\omega)} \tag{8}$$

with

$$g_3^{\alpha\beta}(\omega) = \int_{-\infty}^{E_f} d\epsilon' \int_{-\infty}^{E_f} d\epsilon \frac{n_{\alpha-\sigma}(\epsilon) n_{\beta\sigma}(\epsilon')}{\omega - \epsilon' - \epsilon - i\delta} \tag{9}$$

$$g_1^{\alpha\beta}(\omega) = \int_{-\infty}^{E_f} d\epsilon' \int_{E_f}^{\infty} d\epsilon \frac{n_{\alpha-\sigma}(\epsilon) n_{\beta\sigma}(\epsilon')}{\omega - \epsilon' + \epsilon - i\delta} \tag{10}$$

$n_{\alpha\sigma}(\epsilon)$ is the spin-dependent orbital density of d single-particle valence states

$$n_{\alpha\sigma}(\epsilon) = \sum_{\mathbf{k}n} |C^n_{\alpha\sigma}(\mathbf{k})|^2 \delta(\epsilon - \epsilon^n_{\mathbf{k}})$$

where $C^n_{\alpha\sigma}(\mathbf{k})$ are the expansion coefficients of Bloch single-particle states in terms of localized orbitals. The Faddeev theory [22] is used to determine the total scattering matrix and the resolvent of the many-body system. The hole self-energy turns out to be given by

$$\Sigma^-_{\mathbf{k}n\sigma}(\omega) = \sum_\beta |C^n_{\beta\sigma}(\mathbf{k})|^2 \cdot \left[\sum_\alpha U \frac{1}{N} \sum_{\mathbf{k}'n'}^{empty} |C^{n'}_{\alpha-\sigma}(\mathbf{k}')|^2 - \Sigma^-_{\beta\sigma}(\omega) \right] \tag{11}$$

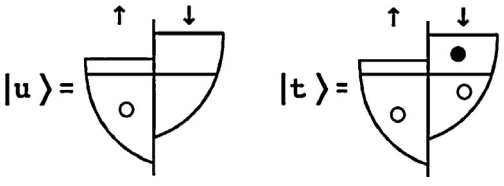

Fig. 3. Pictorial representation of the basis states for the $N-1$ – particle systems. Arrows represent the two different spin channels.

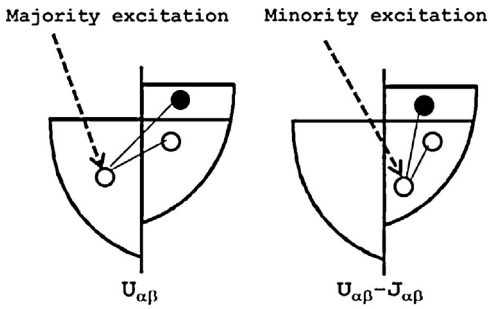

Fig. 4. Schematic representation of the interactions involved in the description of the interacting state with one electron removed from majority- and minority-spin bands in a perfect ferromagnet.

where

$$\Sigma^{-}_{\beta\sigma}(\omega) = \sum_{\alpha} \int_{E_f}^{\infty} d\epsilon \;\; n_{\alpha-\sigma}(\epsilon) \;\; T^{\alpha\beta}_{\mathrm{h-h}}(\omega-\epsilon)\cdot[1+UA^{\alpha\beta}(\omega-\epsilon)]. \tag{12}$$

$A^{\alpha\beta}$ is the quantity related to e–h scattering described by $T^{\alpha\beta}_{\mathrm{h-e}}$ and is determined by a numerical solution of the integral equation described in Ref. [8,10]. The extension to minority spin electrons is straightforward.

In the case of an almost completely filled band the e–h scatterings are very weak and the $T^{\alpha\beta}_{h-e}$ matrix negligibly small: in this case the T-matrix result by Kanamori [23–25] is regained.

As already mentioned 3BS theory provides an intuitive picture of the influence of e–e interaction in the hole or particle excitations, interpreting them in terms of scattering whose efficiency scales with the strength of the e–e repulsion but depends also on the band occupation. As a consequence, according to 3BS scheme it is easy to understand why self-energy may be strongly spin-dependent: in a ferromagnet, where the number of empty states is larger for minority spins than for majority spin ones, the creation of a majority spin hole is followed by scattering processes involving mainly opposite spin electron–hole pairs of intensity proportional to U, while the creation of a minority spin hole involves less intense scattering of strength proportional to $U-J$ (Fig. 4). Self-energy renormalization will then be larger for majority spin states than for minority ones. This is expected to be a general feature and indicates a profound interplay between magnetism and many body effects.

In the same way we easily understand why half occupied bands are most prone to correlation effects and why changes in the band occupation, for instance by doping, may dramatically influence self-energy renormalizations. We will see these effects more clearly in the next paragraph, discussing specific examples and comparing theoretical results with photoemission spectra.

The 3BS hole and particle self-energies are represented diagrammatically in Fig. 5 where the first addendum corresponds to the Kanamori T-matrix result where many-body effects associated to electron Coulomb repulsion are reduced to h–h (e–e) scatterings for the electron removal (addition) process; in the second addendum multiple h–h, e–h and e–e scattering channels come into play.

Before concluding this overview of 3BS theory we want to mention that this approach can be easily extended to describe the shake-up processes that take place when a core hole is photoexcited in the presence of the valence state continuum; in this way it has been possible to provide an interpretation of X-ray photoemission spectra (XPS) from core levels of transition metal and transition metal oxides [26,27,10]. 3BS has also been applied to describe neutral excitation like XAS and XMCD [28]where electrons removed from an inner core state are added to itinerant conduction states. In this case the challenge is to treat on the same footing both the atomistic interactions resulting in multiplet structures of core states and the short range e–e interactions that in the conduction states coexist with hopping from site to site. Moreover, extending the formalism to non equilibrium Green's functions the 3BS approach has been applied also to transport properties of nano-structures [29,30] demonstrating that the finite life time of quasiparticle (associated to the imaginary part of the self-energy) may be responsible of the major quenching factor on the transmittance.

3. Quasiparticle band structure: theory vs experiments

Many body effects modify the energy-versus-momentum relation that applies to non-interacting particles, and quasiparticle band structure may be significantly different from what is deduced within the independent particle picture. Many body interactions may induce also lifetime broadenings which can be observed by ultra-high resolution photoemission studies. In this sense band mapping, i.e. the reduction of the measured spectra to a quasiparticle band structure and its comparison with theoretical results is a powerful tool to investigate many body effects and to validate the very hypothesis of quasiparticle theory.

A theoretical model of the photoemission process is also needed in order to establish a full correspondence between the measured photocurrent and the calculated spectral functions. Different approaches are available to this end, based on three-step or one-step models that describe the photoemission process respectively as a sequence of independent steps (optical excitation of the electron inside the bulk, travel of the excited electron to the surface, escape of the photoelectron into vacuum) [31] or as a single coherent process, where the final state of the photoelectron inside the solid is a time-reversed low energy electron diffraction state [32,33]. In most cases these models are applied assuming a single-particle description of the electron states but many-body effects may be also added in terms of self-energy corrections [34].

We will focus in the following on materials that are known to exhibit non trivial many-body effects such as quasiparticle renormalization/quenching and Mott-Hubbard metal-to-insulator transition.

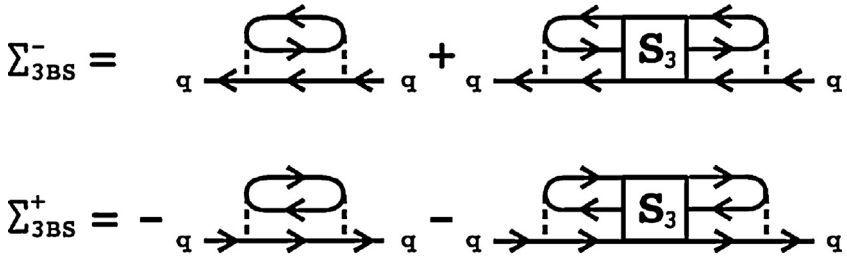

Fig. 5. Diagrammatic representation of $\Sigma^{\pm}$. The box S_3 represents multiple hole and particle scatterings.

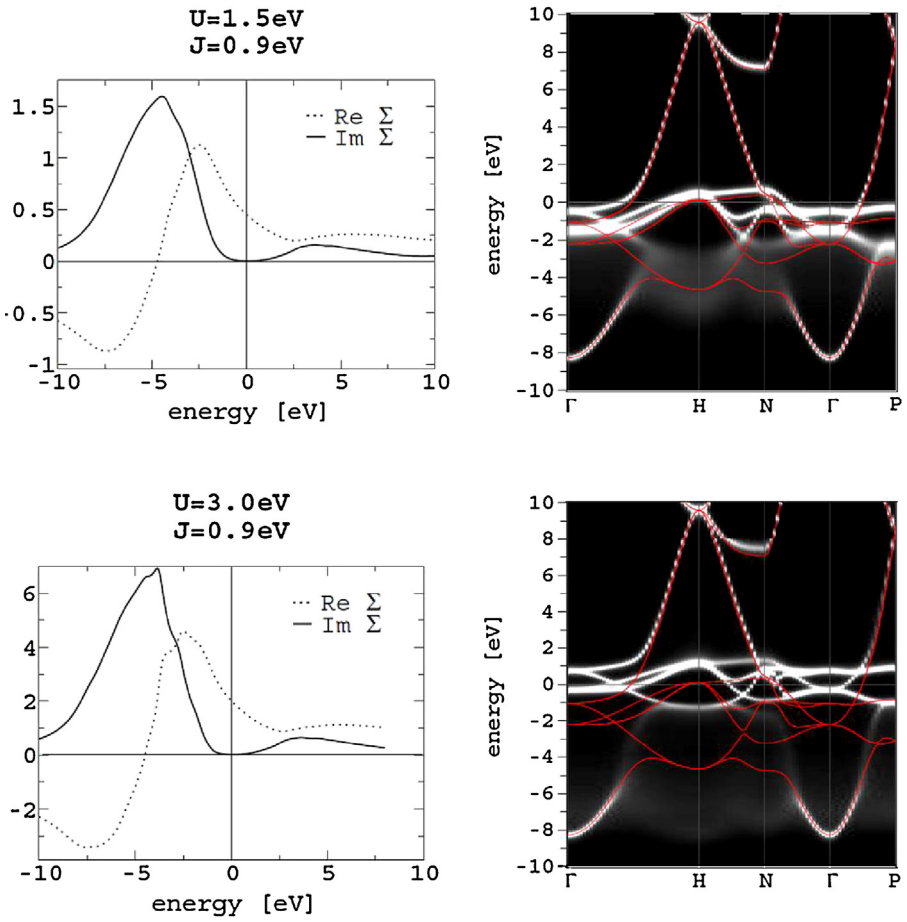

Fig. 6. Self-energy (left) and correlated band structure (right) of bcc iron for two different values of the Hubbard parameter U, for majority spin. The DFT band structure dispersion is also shown (red lines) for reference. (For interpretation of the references to color in this figure legend, the reader is referred to the web version of the article.)

3.1. Transition metals

Late transition metals (TM), iron, cobalt and nickel, are prototypical examples of materials where the itinerant character of valence electrons coexists with local correlations. While these systems can be considered as moderately correlated, still they show some important correlation effects such as the shrinking of the 3*d* band and the formation of non-coherent satellites structures in their photoemission spectrum. If observed down to the very details that are now allowed by modern experimental techniques they look less and less conventional, and despite their importance for nearly all fields of technology, it turns out that we still lack a full quantitative understanding of their electronic properties [35–37].

Let us start our analysis with iron. In Figs. 6 and 7 the self-energy and quasiparticle band structure calculated in the 3BS scheme are reported for two different values of U, namely $U_{dd} = 1.5$ eV and $U_{dd} = 3$ eV. The width of the peaks appearing in the spectral function is essentially defined by the imaginary part of the self-energy, and inversely related to the lifetime of the corresponding quasiparticle.

Consistently with the Fermi liquid theory, $Im\Sigma$ in Figs. 6 and 7 goes to zero near the Fermi energy: in this region of the spectrum we can see well-defined lines of band structure, corresponding to long-lived quasi-particles excitations. Conversely between 3 and 6 eV binding energy $Im\Sigma$ assumes its maximum value, and correspondingly in this region the bands are substantially damped. The effect of the real part of the self-energy is to renormalize quasiparticle energies, shifting the real poles of the Green's function. As a result the electronic states in the region between the Fermi energy and −5 eV, where $Re\Sigma$ is positive, are pushed upwards: the net effect is to shift and shrink the bands, as can be seen in the corresponding spectral functions.

From Figs. 6 and 7 it is also apparent that in the filled part of the spectrum majority spin states are more affected by correlations then minority spin ones, while the reverse is true for empty states. As previously mentioned this is easily understood in the framework of 3BS scheme where the efficiency of the scattering processes depends on the number of states accessible for the scattering itself; for hole states (filled states, probed by direct photoemission) the scattering efficiency depends on the number of empty states, while for particle states (empty states, probed by inverse photoemission) the scattering efficiency depends on the number of filled states. By these arguments and taking into account the spin dependence of the interactions – proportional to U for opposite spins and to $U - J$ for parallel ones – we expect the most effective scattering channels to be those involving three-particle configurations of two different kinds: either a majority spin hole plus a minority spin electron–hole pair, or a minority electron plus a majority spin electron–hole pair, resulting in filled majority and empty minority spin states to be most affected by electron–electron correlation. Finally we notice that increasing U the self-energy increases, still maintaining the same structure: the effects on the band structure remain qualitatively the same but with enhanced importance.

It is interesting to compare the 3BS results with those obtained by DMFT. Both schemes are a non-perturbative solution of the Hubbard model and are expected to describe basically the same physics. Since they are both based on approximations, their comparison may serve as a mutual validation. We consider here iron as a test case and the DMFT results of Ref. [38]. In that paper DMFT has been

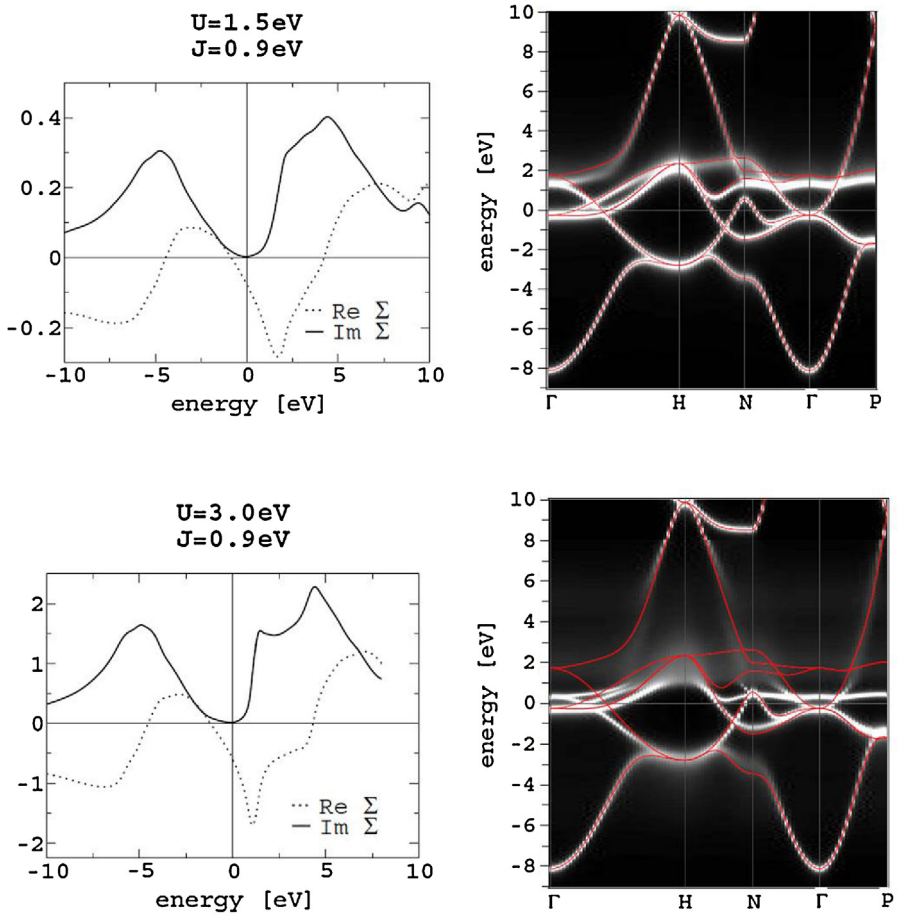

Fig. 7. The same as in Fig. 6 but for minority spin.

applied choosing the spin polarized T-matrix fluctuation exchange (SPTF) as a solver of the impurity problem, an approximation that is believed to be appropriate for transition metals where U is of the same order of magnitude of the band width W and the d band is almost filled (low-density of holes). In this limit 3BS theory can be also reduced to its T-matrix Kanamori form (see previous section) and in the following we will compare both T-matrix and full 3BS results with DMFT-SPTF.

The 3BS and DMFT self-energy for iron are shown in Figs. 8 and 9 First of all we notice that the scale of the self-energy functions is the same, which means that the two methods give similar estimates of the strength of correlation effects; the overall shape of Σ is also comparable, but some differences arise going down to the details. In particular it is interesting to observe that the position of the maxima of $Im\Sigma_{DMFT}$ occur at the same energy of T-matrix $Im\Sigma_{3BS}$, while the maxima of the $Im\Sigma_{3BS}$ obtained using the complete 3BS theory are shifted to higher values. Since maxima in the imaginary part of the self-energy appear as wide maxima in the spectral function, signalling the presence of incoherent short-lived satellite excitations, we expect these features of DMFT and 3BS self-energies to affect spectral features.

The sum of spin-resolved spectral functions (3) over k-vector and band index n, namely the spin-resolved density of quasiparticle states, is shown in Fig. 10. As expected the density of states calculated in DMFT is quite similar to one obtained by 3BS in the T-matrix approximation with a satellite peak around −7.5 eV, while the full 3BS theory sets the satellite position at a lower binding energy.

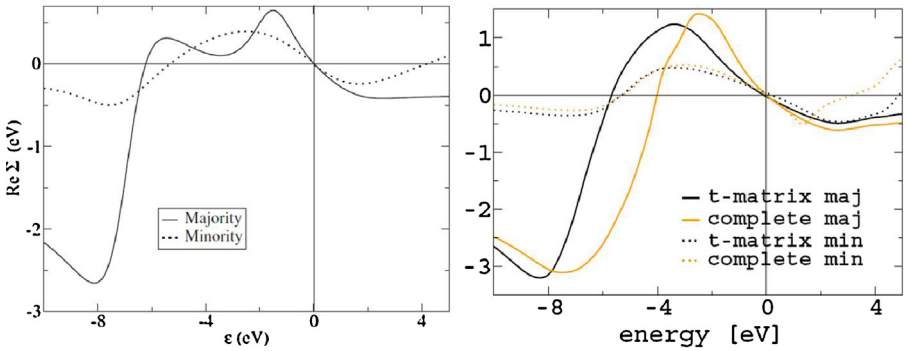

Fig. 8. Real part of the self-energy of bcc bulk iron: DMFT [38] (left) and 3BS (right) results, for both spins.

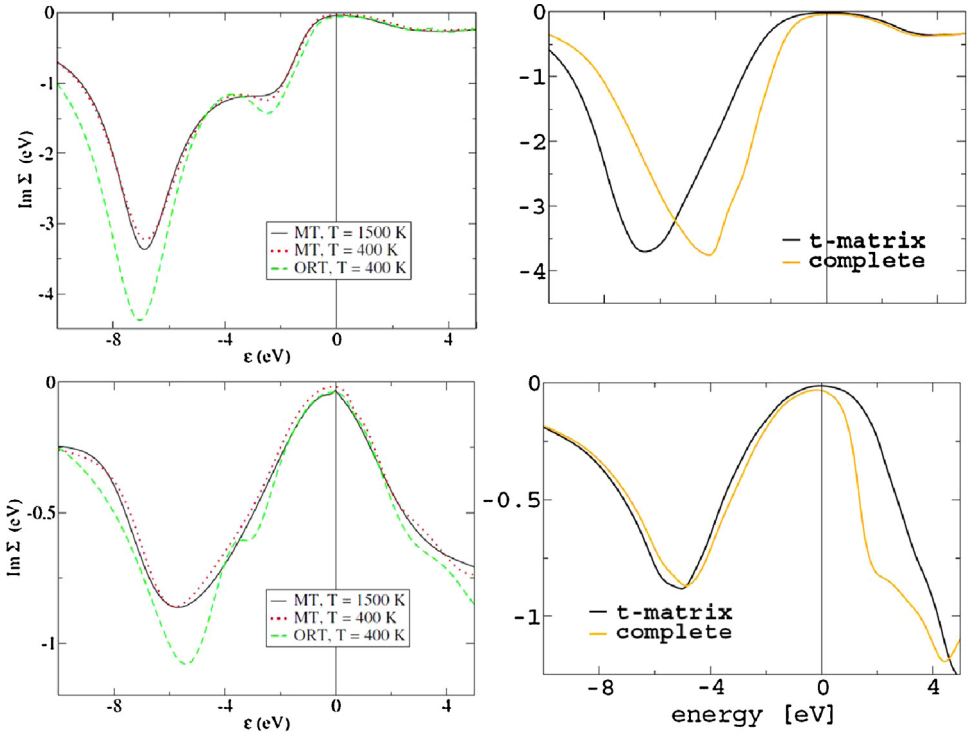

Fig. 9. Imaginary part of the self-energy of bcc bulk iron $-Im\Sigma$: comparison between DMFT [38] (left) and 3BS (right). Majority spin is shown at the top, minority spin at the bottom. For DMFT the various lines refer to different sets of correlated orbitals and different temperatures; for 3BS we show both the complete self-energy and the T-matrix contribution.

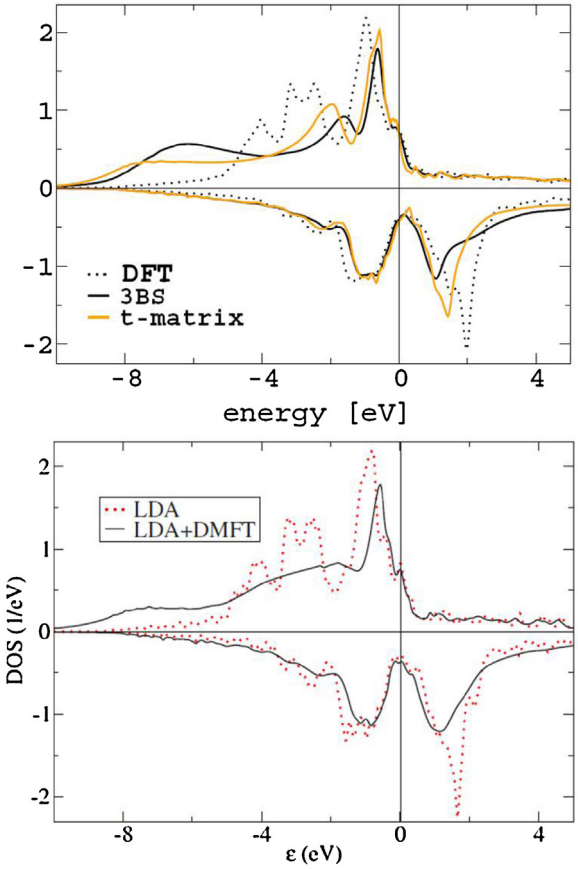

Fig. 10. Spin-resolved (top: majority spin; bottom: minority spin) 3BS (left) and DMFT [38] (right) correlated density of states of bcc iron. For 3BS both the complete self-energy (black) and the T-matrix approximation (yellow) are shown. The bare DFT result (dots) is also reported for reference. (For interpretation of the references to color in this figure legend, the reader is referred to the web version of the article.)

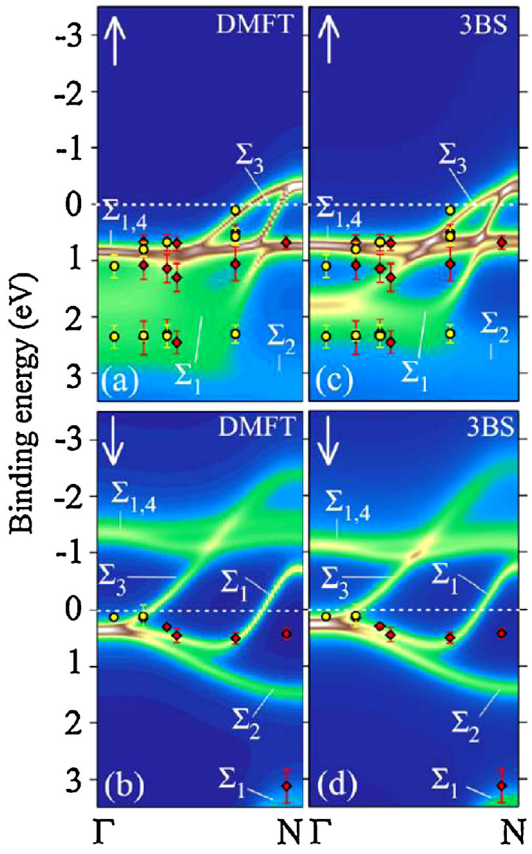

Fig. 11. Spectral function of Fe(1 1 0) obtained by 3BS and DMFT compared with photoemission data reported as symbols. From Ref. [35].

We want to stress that here the analysis is predominately methodological, showing how specific theoretical approaches and approximations affect the final result. The comparison with experimental data is not the point and we only register that starting from the same input (DFT band structure and $U-J$ parameters) full 3BS theory predicts the satellite structure at a lower binding energy than DMFT-SPTF. Since experimentally in iron no clear satellite structure can be distinguished except at very low binding energies [39,40] this observation may suggest that full 3BS approach that takes care of all (h–h, e–e and also e–h) scattering channels should be preferred to its T-matrix counterpart and to DMFT – SPTF. It would be very instructive to extend this detailed comparison between 3BS and DMFT to calculations performed within DMFT using different impurity solvers.

As shown in Figs. 6, 7 increasing the values of U from 1.5 to 3 eV the incoherent short-lived excitations that exist around H point move down from −4 to −8 eV and we may then identify $U = 1.5$ eV as the optimal value as far as the satellite energy position is concerned; we may then use this value in the comparison with ARPES spectra in the whole energy range, from the bottom of the valence band up to the Fermi energy.

Several ARPES studies have been done in the past for iron and other transition metals [41–43] but here we refer mainly to the recent spin-resolved data of Refs. [35–37] where photoemission spectra from the Fe(1 1 0) surface have been taken in normal emission and with both p- and s-polarized photons. The information on light polarization is essential in order to discriminate between states of different symmetry. The measured photo-current in fact is given by the spectral function modulated by the matrix elements of the photon–solid interaction; these can be calculated within different approximations and have basically the effect of modifying the intensity of the peaks observed in the photoemission spectrum. The one-step model is the most refined approach in which the whole process of photoemission, that is the excitation of the photoelectron, its transport within the solid and its escape through the surface into the vacuum, is treated as a single coherent process [44,45].

The analysis of the above mentioned experimental spectra within the one-step model has been reported in Refs. [35–37] and shown for majority spin electrons in Fig. 11. It is however instructive to analyze the spectra also in terms of simple symmetry related on/off selection rules [21]. This analysis is shown in Figs. 12 and 13 where the photoemission spectra obtained for majority spins in s- and p-polarization is compared with both single-particle and 3BS results.

For majority spin, the main feature in the experimental p-polarization spectra is a peak close to the Fermi energy, dispersing from ∼1.1 to 0.8 eV binding energy going from Γ to N. This peak can be assigned to nearly degenerate Σ_1 and Σ_4 bulk states and its

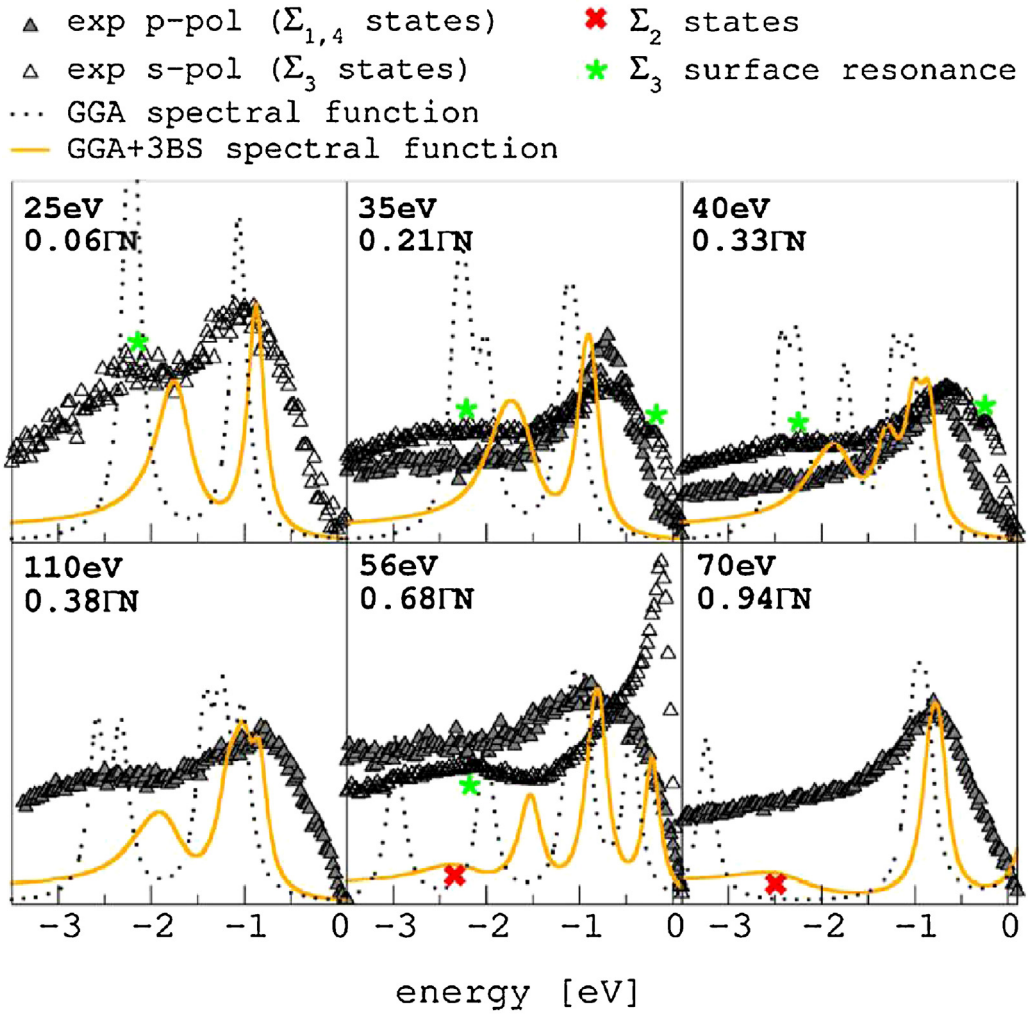

Fig. 12. Comparison between photoemission spectra of Ref. [35], bare DFT bulk spectral function and DFT + 3BS bulk spectral function of bcc iron, for majority spin. The various panels refer to different incoming photon energies, corresponding to different points of the Brillouin zone along the $\Gamma - N$ direction. We have explicitly marked Σ_2 states appearing in the spectral functions, which are experimentally forbidden, and surface resonances appearing in the experiment but not included in the theoretical calculation. From Ref. [21].

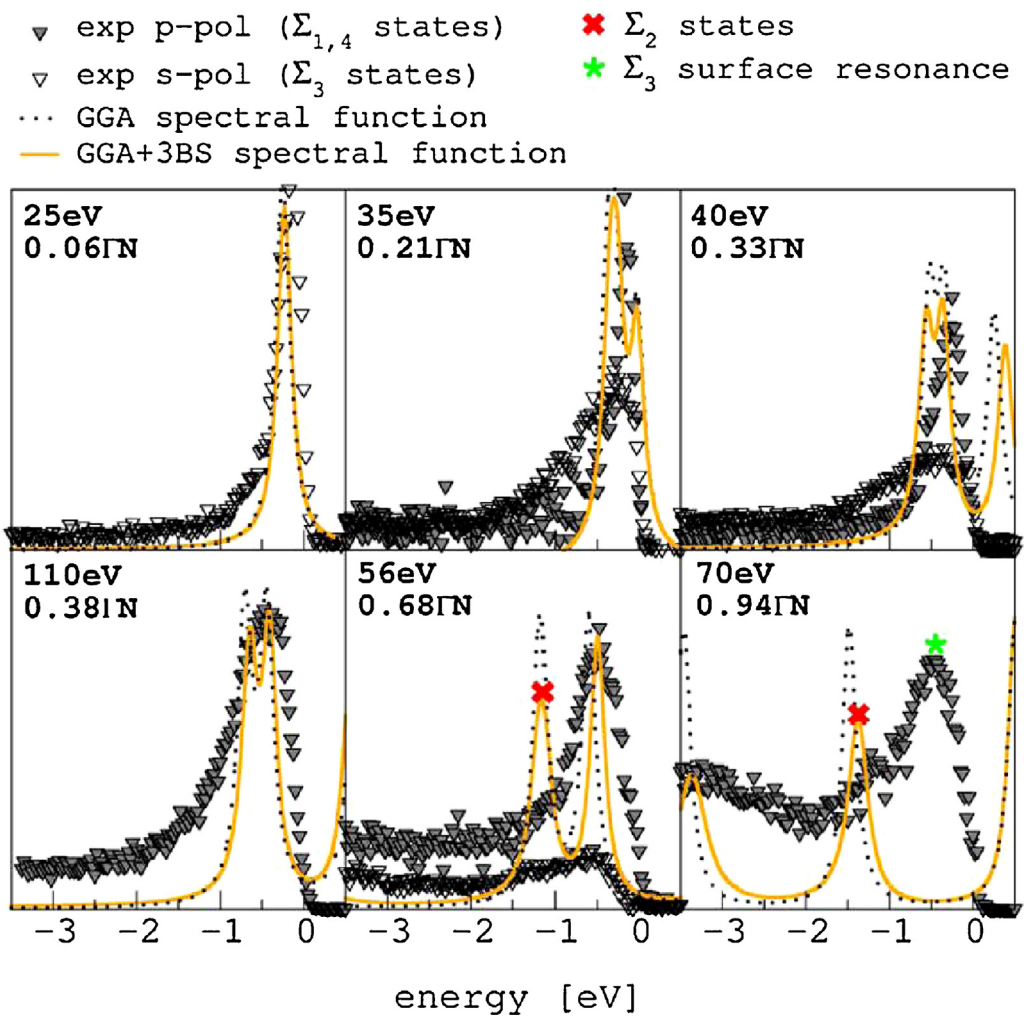

Fig. 13. The same as in Fig. 12 but for minority spins.

position is systematically improved by 3BS corrections with respect to the bare DFT band calculation. The s-polarization spectra show two additional features: a broad non-dispersive peak at ∼2.2 eV and a shoulder near the Fermi energy which can be associated to a surface state [21].

For minority spin, according to DFT calculations three degenerate bands are present at the Γ point close to the Fermi energy, together with a surface resonance. One of the bands has Σ_2 symmetry thus is not visible in the experiment; of the remaining two, the Σ_3 band crosses the Fermi level at about 1/3 Γ*N*, while the one at about 4/5 Γ*N*; at this point the underlying surface contribution becomes visible. In the case of minority spin no significant differences arise between DFT and DFT + 3BS calculation and they both agree with the experiment.

We may conclude this analysis by noticing that iron is a paradigmatic example of quasiparticle renormalization induced by local e–e interactions: self-energy corrections modify the energy position and the dispersion of single-particle eigenvalues giving rise to well defined spectral features that correspond to long lived excitations. This is true also of nickel but, surprisingly enough not of cobalt where due many-body effects no sharp quasiparticle peaks exist for binding energies larger than 2 eV.

The results for cobalt obtained by 3BS theory are shown in Fig. 14 where the *k*-resolved hole spectral function are plotted along the Γ – *M* direction calculated within the 3BS approach ($U = 2.1$ eV, $J = 0.8$ eV). No sharp peak exists below 2.0 eV in agreement with experimental findings, and the spectral functions exhibit only a uniform background. Because of e–e interaction the components of the many-body state with $N-1$ particles remain then coherent only over a very short time and the time evolution of the state with one removed particle cannot be reduced to a quasiparticle propagation. The dominance of incoherent excitation is due to the large value of the imaginary part of the self-energy in this energy region. The reason why these effects are so much stronger in cobalt than in iron and nickel in spite of the similar strength of the screened on-site e–e interaction has to do with the band occupation. In the extreme case of a completely filled band, where no e–h pairs can be added, correlation effects are absent, irrespectively of the strength of the e–e interaction. This is the case of copper, the only metal of the 3*d* transition series where band theory gives a full account of photoemission data. In all the other cases we expect self-energy corrections to increase – for given *U* and *J* – with an increasing number of unoccupied *d* states: in the same way as in atoms, where the complexity of the multiplet structure depends on the shell occupation, the number and mixing of configurations is larger when the valence band has a high density of holes. This is evident in the 3BS approach where the e–h and e–e scattering efficiency depends directly on the number of empty d states necessary for the creation of excited configurations.

A detailed comparison between calculated and measured lifetimes (Fig. 15) confirms the peculiarity of cobalt among the other 3*d* transition metals: in cobalt the life time of the hole excitations is much lower than in Ni and Fe and quasiparticle sates are quenched in a wide energy region close to the Fermi energy. This is rather

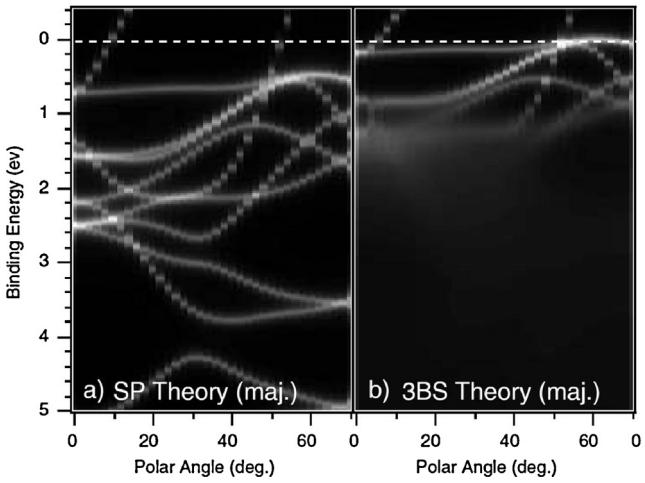

Fig. 14. (a) Quasiparticle spectral function for majority spin in hcp Co calculated by 3BS approach. (b) Corresponding single-particle band structure. From Ref. [11].

weird behaviour for a conventional metal, that contradicts the prediction of Fermi liquid theory about low-energy excitations and their one-to-one correspondence with single particle states.

3.2. Transition metal oxides

The competition between inter-site hopping and on-site electron–electron repulsion dominates the physics of transition metal oxides [46]. Standard band theory based on the independent particle approach predicts these large gap insulators to be metallic in the paramagnetic phase and fails in reproducing the bandwidth and satellite structures observed in the experiments.

The Hubbard mechanism that inhibits double occupancies of sites, thus reducing the ability of electrons to jump from place to place, is at the core of the insulating phase of paramagnetic transition metals oxides. If Coulomb repulsion dominates, electrons have to avoid each other and if there are as many sites as electrons the "electron traffic" comes to a complete stand still: we may say that "Mott insulators are the incarnation of rush hour traffic in the world of electrons" [47]. Even if the physical origin of the Mott-Hubbard metal-to-insulator transition is qualitatively as simple as that, the solution of the many-body problem associated to it is anything but trivial.

The first attempt to provide a detailed description of the quasiparticle band structure of a transition metal oxide adding Hubbard correlation to DFT band structure dates back to the early 90's when the electronic structure of NiO inclusive of many-body effects has been calculated within 3BS theory [9], reproducing both the insulating gap, the satellite structure and the orbital character of the valence band edge. This work was followed much later by a DMFT study [48] showing again quite similar results. Other studies have been presented since then on NiO and other transition metal oxides, based either on more refined choices of DFT functionals [49] or on many-body perturbative (GW) expansions [50,51].

Fig. 16 shows the results for MnO obtained using two different theoretical approaches, namely cluster perturbation theory (CPT) [19] and DMFT [52] compared with direct and inverse photoemission data [53]. As anticipated in the introduction, CPT belongs to the class of quantum cluster approaches that solve the problem of many interacting electrons in an extended lattice by approaching first the many body problem in a subsystem of finite size – a cluster – and then embedding it within the infinite medium. CPT shares this strategy with other approaches such as cellular dynamical mean field theory [15] where the embedding procedure is variationally optimized. One of the advantage of QC approaches is to better describe the k-dependence of self-energy renormalization.

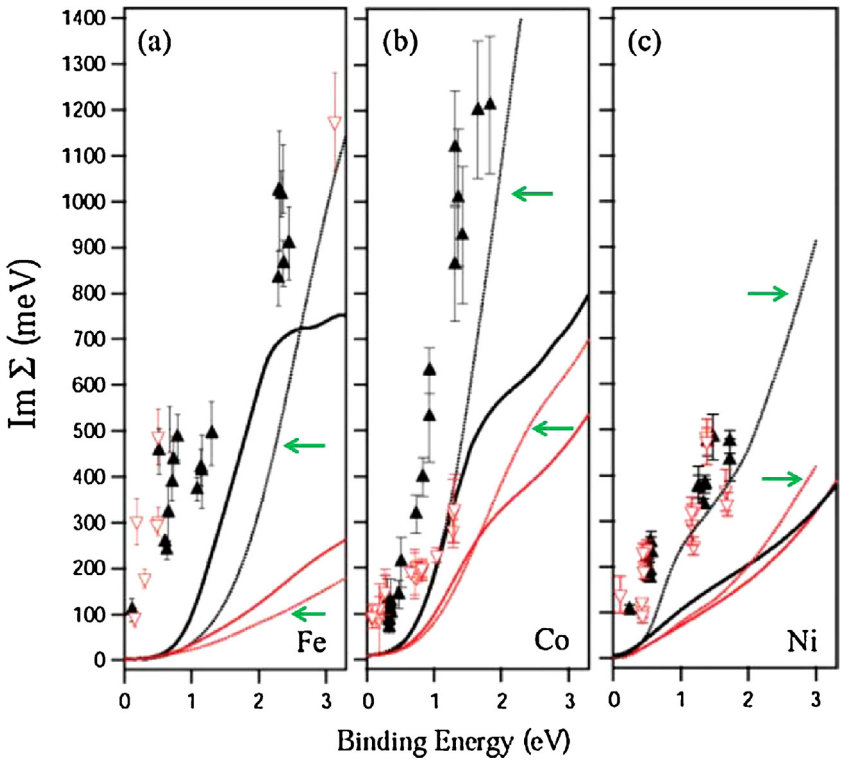

Fig. 15. Comparison between the experimental (symbols) and theoretical (lines) imaginary parts of the self-energies of (a) Fe(1 1 0), (b) Co(0 0 0 1), and (c) Ni(1 1 1) for majority (black) and minority (red) spin electrons. The theoretical calculations correspond to $Im\Sigma_{DMFT}$ (thick solid lines) and to $Im\Sigma_{3BS}$ (thinner lines marked with green arrows) From Ref. [37] (For interpretation of the references to color in this figure legend, the reader is referred to the web version of the article.).

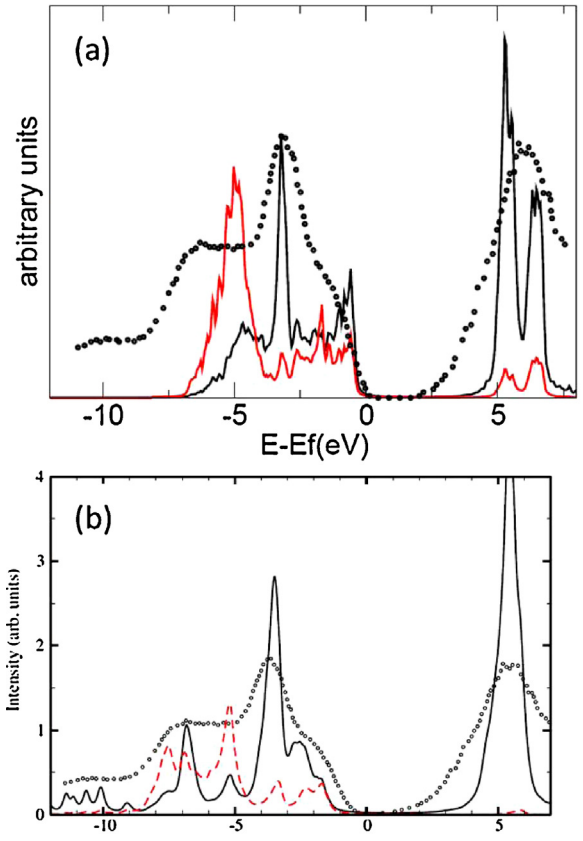

Fig. 16. (a) Orbital resolved density of quasiparticle states calculated according to CPT compared with the experimental XPS and BIS data (circles) of Ref. [53]. Black (red) line is for TM *d* (Oxygen *p*) orbital contribution. Adapted from [19]. (b) The same results obtained by DMFT and reported in Ref. [52] (For interpretation of the references to color in this figure legend, the reader is referred to the web version of the article.).

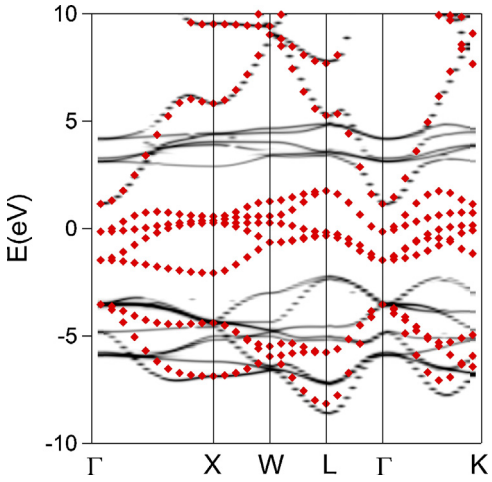

Fig. 17. *k*-Resolved spectral functions describing the quasiparticle band structure of MnO for $U = 9$ calculate by CPT [19].

However their application to real materials has been up to now rather limited for the several difficulties mainly of numerical character (see Section 4 for more details).

We observe that in Fig. 16 both approaches reproduce correctly the gap value as well as most of the spectroscopic structures. In CPT no evidence is found of structures below the valence band bottom that are observed in photoemission experiments; this might well be due to the approximations of the method but it is worth recalling that the origin of satellites features in MnO has been somewhat controversial in the literature attributing them either to intrinsic [53] or extrinsic effects [54]. The quasiparticle band structure of MnO is shown in Fig. 17. We notice that the Mn *d* band that in the absence of correlation crosses the Fermi level is now split in lower and upper Hubbard bands.

4. Summary, open problems and outlook

We have discussed how single-particle band structure can be augmented by local repulsive interaction among electrons. 3BS approach is an efficient way to describe short range e–e correlations in model systems and real materials in all correlation regimes. It describes incoherent states, quasiparticle renormalization and quasiparticle quenching as well as Mott-Hubbard metal-to insulator transition. Within 3BS it is possible to obtain an intuitive interpretation of the effects of electron correlation on one electron removal/addition energies and to understand why minority spin valence states are less influenced by e–e interaction than majority spin ones, leading to a spin dependent quasiparticle renormalization.

Since all many-body approaches to real materials rely on drastic approximations, it is extremely useful to perform accurate comparison between the outcomes of different methods. We have analyzed the results of 3BS and DMFT showing that the agreement between the two approaches is rather good but that it depends on the choice of the impurity solver adopted in the DMFT calculation. This might be a general result and suggests that the choice of different details in the implementation of a theoretical method (as the impurity solver in this case) should be checked and made clear.

Other open questions exist that are common to all the methods that add local e–e interaction to band single particle band.

The starting point issue. It is known that the DFT band structure is in many cases a good zero-order approximation to the excitation spectrum of a solid, and it seems reasonable to use it as a starting point for the inclusion of correlation effects: the implicit assumption is that, among all the many-body terms responsible for correlations, the on-site Coulomb repulsion is the one which needs to be treated explicitly. But which specific mean-field theory should be chosen as a starting point? Hartree-Fock theory would be the method of election to treat Coulomb interaction at first order, with a complete control over the successive higher order terms. Nevertheless the state of the art method to compute band structures is DFT, and this is the commonly preferred starting point for the inclusion of correlation effects as well. Moreover another and more relevant reason why DFT should be preferred is that most of the approaches used to go beyond the single particle picture, and most of the current implementations, renormalize the eigenvalues leaving the eigenfunctions unaltered: they therefore need the best possible single particle wavefunctions that is commonly believed to be provided by DFT. On the other hand choosing DFT gives rise to the problem of which exchange correlation functional is to be selected among the vast variety of proposed functionals, including Hybrids [55], LDA + U [56,57], self-interaction corrected [58], exact exchange [59], etc.

The starting point issue may be mitigated by introducing some sort of self-consistency between the input and output charge density as presently implemented within DMFT [60].

The double counting issue. The other problem is the subtraction of any double counting of the electron–electron interaction included in the DFT calculation via the exchange-correlation potential. Since DFT describes, although in a mean field fashion, the whole electron-electron interaction, and in the Hubbard model one-site Coulomb repulsion is explicitly considered, when we put the two worlds together in a unique Hamiltonian of the type of Eq. 1 we found contributions due to the additional Hubbard term that have

already been included in the DFT solution, and which should be removed in order to avoid to count them twice. Generally this is done by subtracting a double-counting term from the self-energy, however such a correction is not unique and its choice represents an open question. In many instances the double counting is taken into account shifting the real part of each orbital self-energy in such a way that their average passes through zero at the Fermi energy. This means that DFT is assumed to properly describe the Fermi surface of the system, which is left identical to that of its uncorrelated counterpart. This result can be reasonable in the case of transition metals, but would be questionable for more strongly correlated materials such as high T_c superconductors; a whole branch of research indeed is involved in the calculation of the complicated Fermi surfaces of strongly correlated materials [61–63].

The choice of U and J. Another issue is the choice of U and J parameters. In the past – and also now in many cases – they are treated as tunable parameters and modified to fix an experimental feature (typically to reproduce the measured satellite energy position) and then used to predict other spectral structures. More recently various techniques have been proposed to calculate them as orbital-dependent screened Coulomb and exchange integrals [64,65], including even their energy dependence [66,67] or constructing a novel class of self-energy functionals (GW+DMFT) [68,69]. These are only few of the many attempts that go in the direction of building ab-initio many-body approaches for real materials, a very active and promising research field.

We have confined our review to the most simple highly correlated solids, neglecting for instance the vast class of more complex materials such as oxides, cuprates, pnictides, etc. that have been the object of many theoretical and experimental studies in the last decades. More recently huge attention has been devoted to the group of materials that go under the name of topological insulators. The role of topology in material science has been one of the major discoveries of the past decades. In these insulating systems the non-dissipative current carried by gapless edge states owes its robustness to a bulk topological feature described by non-zero value of given invariants. In most cases topological characteristics are defined assuming the electrons to be non-interacting and an important issue is to understand how e–e repulsion may affect topological order and influence the physical observables related to it [70,71]. The field of interacting topological insulators is attracting growing interest and the definition of theoretical and computational tools to evaluate topological invariants in the presence of e–e interaction will require in the future dedicated efforts by the theoretical community.

References

[1] R. Martin, Electronic Structure: Basic Theory and Practical Methods, Cambridge University Press, 2004.
[2] G. Kotliar, S.Y. Savrasov, K. Haule, V.S. Oudovenko, O. Parcollet, C.A. Marianetti, Rev. Mod. Phys. 78 (2006) 865.
[3] A. Georges, G. Kotliar, W. Krauth, M.J. Rozenberg, Rev. Mod. Phys. 68 (1996) 13.
[4] K.M. Ho, J. Schmalian, C.Z. Wang, Phys. Rev. B 77 (2008) 073101.
[5] X. Deng, L. Wang, X. Dai, Z. Fang, Phys. Rev. B 79 (2009) 075114.
[6] G. Borghi, M. Fabrizio, E. Tosatti, Phys. Rev. B 90 (2014) 125102.
[7] J.-I. Igarashi, P. Unger, K. Hirai, P. Fulde, Phys. Rev. B 49 (1994) 16181.
[8] C. Calandra, F. Manghi, Phys. Rev. B 50 (1994) 2061.
[9] F. Manghi, C. Calandra, S. Ossicini, Phys. Rev. Lett. 73 (1994) 3129.
[10] F. Manghi, V. Bellini, C. Arcangeli, Phys. Rev. B 56 (1997) 7149.
[11] S. Monastra, F. Manghi, C.A. Rozzi, C. Arcangeli, E. Wetli, H.-J. Neff, T. Greber, J. Osterwalder, Phys. Rev. Lett. 88 (2002) 236402.
[12] T. Maier, M. Jarrell, T. Pruschke, M.H. Hettler, Rev. Mod. Phys. 77 (2005) 1027.
[13] M.H. Hettler, A.N. Tahvildar-Zadeh, M. Jarrell, T. Pruschke, H.R. Krishnamurthy, Phys. Rev. B 58 (1998) R7475.
[14] G. Kotliar, S.Y. Savrasov, G. Pálsson, G. Biroli, Phys. Rev. Lett. 87 (2001) 186401.
[15] S.S. Kancharla, B. Kyung, D. Sénéchal, M. Civelli, M. Capone, G. Kotliar, A.-M.S. Tremblay, Phys. Rev. B 77 (2008) 184516.
[16] C. Gros, R. Valentí, Phys. Rev. B 48 (1993) 418.
[17] D. Sénéchal, D. Perez, M. Pioro-Ladrière, Phys. Rev. Lett. 84 (2000) 522.
[18] F. Manghi, F. Petocchi, Phys. Scr. 89 (2014) 075802.
[19] F. Manghi, J. Phys.: Condens. Matter 26 (2014) 015602.
[20] R. Eder, Phys. Rev. B 78 (2008) 115111.
[21] V. Boni, A 3BS Approach to Electron–Electron Correlations in Solids (Ph.D. thesis), Univ. of Modena and Reggio E, 2010.
[22] L.D. Faddeev, Sov. Phys. JETP 12 (1963) 275.
[23] J. Kanamori, Prog. Theor. Phys. 30 (1963) 275 http://ptp.oxfordjournals.org/content/30/3/275.full.pdf+html
[24] A. Liebsch, Phys. Rev. B 23 (1981) 5203.
[25] C. Calandra, F. Manghi, Phys. Rev. B 45 (1992) 5819.
[26] C.A. Rozzi, F. Manghi, C. Arcangeli, Phys. Rev. B 62 (2000) R4774.
[27] C.A. Rozzi, F. Manghi, C. Calandra, Phys. Rev. B 72 (2005) 125106.
[28] L. Pardini, V. Bellini, F. Manghi, J. Phys.: Condens. Matter 23 (2011) 215601.
[29] A. Ferretti, A. Calzolari, R. Di Felice, F. Manghi, M.J. Caldas, M.B. Nardelli, E. Molinari, Phys. Rev. Lett. 94 (2005) 116802.
[30] A. Ferretti, A. Calzolari, R. Di Felice, F. Manghi, Phys. Rev. B 72 (2005) 125114.
[31] P.J. Feibelman, D.E. Eastman, Phys. Rev. B 10 (1974) 4932.
[32] J. Pendry, Surf. Sci. 57 (1976) 679.
[33] J. Braun, Rep. Prog. Phys. 59 (1996) 1267.
[34] J. Minár, J. Braun, H. Ebert, J. Electron Spectrosc. Relat. Phenom. 190 (Part B) (2013) 159, Recent Advances in Hard X-ray Photoelectron Spectroscopy (HAXPES).
[35] J. Sánchez-Barriga, J. Fink, V. Boni, I. Di Marco, J. Braun, J. Minár, A. Varykhalov, O. Rader, V. Bellini, F. Manghi, H. Ebert, M.I. Katsnelson, A.I. Lichtenstein, O. Eriksson, W. Eberhardt, H.A. Dürr, Phys. Rev. Lett. 103 (2009) 267203.
[36] J. Sánchez-Barriga, J. Minár, J. Braun, A. Varykhalov, V. Boni, I. Di Marco, O. Rader, V. Bellini, F. Manghi, H. Ebert, M.I. Katsnelson, A.I. Lichtenstein, O. Eriksson, W. Eberhardt, H.A. Dürr, J. Fink, Phys. Rev. B 82 (2010) 104414.
[37] J. Sánchez-Barriga, J. Braun, J. Minár, I. Di Marco, A. Varykhalov, O. Rader, V. Boni, V. Bellini, F. Manghi, H. Ebert, M.I. Katsnelson, A.I. Lichtenstein, O. Eriksson, W. Eberhardt, H.A. Dürr, J. Fink, Phys. Rev. B 85 (2012) 205109.
[38] A. Grechnev, I. Di Marco, M.I. Katsnelson, A.I. Lichtenstein, J. Wills, O. Eriksson, Phys. Rev. B 76 (2007) 035107.
[39] D.E. Eastman, F.J. Himpsel, J.A. Knapp, Phys. Rev. Lett. 44 (1980) 95.
[40] S. Hüfner, S.-H. Yang, B.S. Mun, C.S. Fadley, J. Schäfer, E. Rotenberg, S.D. Kevan, Phys. Rev. B 61 (2000) 12582.
[41] A.M. Turner, A.W. Donoho, J.L. Erskine, Phys. Rev. B 29 (1984) 2986.
[42] J. Schäfer, M. Hoinkis, E. Rotenberg, P. Blaha, R. Claessen, Phys. Rev. B 72 (2005) 155115.
[43] J. Schäfer, D. Schrupp, E. Rotenberg, K. Rossnagel, H. Koh, P. Blaha, R. Claessen, Phys. Rev. Lett. 92 (2004) 097205.
[44] P.J. Feibelman, D.E. Eastman, Phys. Rev. B 10 (1974) 4932.
[45] J. Pendry, Surf. Sci. 57 (1976) 679.
[46] M. Imada, A. Fujimori, Y. Tokura, Rev. Mod. Phys. 70 (1998) 1039.
[47] J. Zaanen, 2011. Available from: arXiv:1012.5461
[48] J. Kuneš, V.I. Anisimov, A.V. Lukoyanov, D. Vollhardt, Phys. Rev. B 75 (2007) 165115.
[49] A.I. Lichtenstein, M.I. Katsnelson, Phys. Rev. B 57 (1998) 6884.
[50] F. Aryasetiawan, O. Gunnarsson, Phys. Rev. Lett. 4 (1995) 3221.
[51] S. Massidda, A. Continenza, M. Posternak, A. Baldereschi, Phys. Rev. B 5 (1997) 13494.
[52] P. Thunström, I. Di Marco, O. Eriksson, Phys. Rev. Lett. 109 (2012) 186401.
[53] J. van Elp, R.H. Potze, H. Eskes, R. Berger, G.A. Sawatzky, Phys. Rev. B 44 (1991) 1530.
[54] A. Fujimori, N. Kimizuka, T. Akahane, T. Chiba, S. Kimura, F. Minami, K. Siratori, M. Taniguchi, S. Ogawa, S. Suga, Phys. Rev. B 42 (1990) 7580.
[55] A.D. Becke, J. Chem. Phys. 98 (1993) 1372.
[56] V.I. Anisimov, J. Zaanen, O.K. Andersen, Phys. Rev. B 44 (1991) 943.
[57] K. Karlsson, F. Aryasetiawan, O. Jepsen, Phys. Rev. B 81 (2010) 245113.
[58] A. Svane, O. Gunnarsson, Phys. Rev. Lett. 65 (1990) 1148.
[59] T. Kotani, Phys. Rev. B 50 (1994) 14816.
[60] F. Lechermann, A. Georges, A. Poteryaev, S. Biermann, M. Posternak, A. Yamasaki, O.K. Andersen, Phys. Rev. B 74 (2006) 125120.
[61] K. Schonhammer, O. Gunnarsson, Phys. Rev. B 37 (1988) 3128.
[62] S. Monastra, F. Manghi, C. Ambrosch-Draxl, Phys. Rev. B 64 (2001) 020507.
[63] A. Paramekanti, E. Zhao, Phys. Rev. B 75 (2007) 140507.
[64] M. Cococcioni, S. de Gironcoli, Phys. Rev. B 71 (2005) 035105.
[65] H.J. Kulik, M. Cococcioni, D.A. Scherlis, N. Marzari, Phys. Rev. Lett. 97 (2006) 103001.
[66] R. Sakuma, F. Aryasetiawan, Phys. Rev. B 87 (2013) 165118.
[67] T. Miyake, F. Aryasetiawan, Phys. Rev. B 77 (2008) 085122.
[68] S. Biermann, F. Aryasetiawan, A. Georges, Phys. Rev. Lett. 90 (2003) 086402.
[69] J.M. Tomczak, S. Biermann, Europhys. Lett. 86 (2009) 37004.
[70] V. Gurarie, Phys. Rev. B 83 (2011) 085426.
[71] F. Grandi, F. Manghi, O. Corradini, C.M. Bertoni, A. Bonini, N. J. Phys. 17 (2015) 023004.